RSC Advances

ROYAL SOCIETY OF CHEMISTRY

www.rsc.org/advances

Performance improvement of activated nanoporous carbon supported gold catalyst as anode for direct borohydride-hydrogen peroxide fuel cell

Jing Liu, Qinglan Zhao, Chun Wu, Yi Wang, Wei wei, Xianyou Wang*, Lanhua Yi

Key Laboratory of Environmentally Friendly Chemistry and Applications of Ministry of Education, School of Chemistry, Xiangtan University, Hunan Xiangtan 411105, China

Abstract: The activated nanoporous carbon (A-NPC) has been synthesized via KOH activation of a nanoporous carbon (NPC) prepared by template metal-organic framework-5 (MOF-5), and it is firstly used as anode electrocatalyst carrier of Au nanoparticles in borohydride-hydrogen peroxide fuel cell (DBHFC). The samples are characterized by N_2 adsorption-desorption isotherm, transmission electron microscopy (TEM), X-ray diffraction (XRD), cyclic voltammetry (CV), chronopotentiometry (CP), chronoamperometry and fuel cell test. It has been found that the A-NPC achieves a surface area up to 2296 m^2 g^{-1} and a pore volume of 1.59 cm^3 g^{-1}. The mean particle size of Au crystallites dispersed uniformly on the surface of A-NPC carrier is only 2.9 nm. Besides, the peak current density for direct borohydride oxidation of the Au/A-NPC (49.1 mA cm^{-2}) is 13.6% higher than that of the untreated NPC supported Au (43.2 mA cm^{-2}), and 63.1% than that of commercial Vulcan XC-72R supported Au (30.1 mA cm^{-2}). The DBHFC using the Au/A-NPC as anode electrocatalyst can obtain a maximum power density of 48.2 mW cm^{-2} at 25 ^oC.

Keywords: gold catalyst; metal-organic framework; activated nanoporous carbon; carrier; direct borohydride-hydrogen peroxide fuel cell

* **Corresponding author:** Xianyou Wang Tel: +86 731 58292060; fax: +86 731 58292061.
E-mail address: wxianyou@yahoo.com (X. Wang).

1. Introduction

DBHFC has received considerable attention over the past decade as potential power source candidate. Since its unique advantages, e.g. avoidance of CO poisoning, high theoretical open circuit voltage (OCV) of 3.01 V and high energy density (9.3 Wh g^{-1} of $NaBH_4$).[1-5] Nevertheless, the commercial deployment of DBHFC is still hindered by the costs of its main constitutive materials, including the noble metals-based catalysts and the expensive fuel.[6,7] One of the most realistic approaches to solve the cost factor is to develop a cost-efficient anode electrocatalyst that is able to enhance the electrocatalytic activity for BH_4^- oxidation and depress unwanted borohydride hydrolysis which decreases the fuel utilization. To date, there are two directions to improve the anode catalysts: firstly, exploring the lower-cost substitutes (e.g. Ni and Cu) and developing binary alloy,[8-10] and secondly, employing the novel carrier materials.[11-14] The latter is a favourable scenario that many researchers have investigated, and the recent studies have revealed that the carriers with advanced properties can not only maximize the availability surface area of the catalytic particles, but also exhibit a synergistic effect on the activity and durability of catalysts. Additionally, the degree of alloying, the mass transport properties, and electronic conductivity of the catalytic layer are also affected by the chosen carrier material.[12] As well known, the current hot novel carriers are carbon nanotubes,[15] carbon xerogel,[16] carbon nanofibers,[17] graphene,[18] and metal oxides.[19] However, these carbon materials are expensive to obtain, whereas metal oxides often suffer from low conductivity and specific surface area.[20] On the contrary, activated carbon with quite a few unique characteristics, such as high surface area, bulk porosity, various surface chemical properties, and simple

preparation process, has attracted tremendous interest as a promising carrier of electrocatalyst for fuel cells.[21-23]

Metal-organic frameworks (MOFs), which are emerging as a new class of crystalline porous materials with multiple functionalities, have been extensively used for gas separation and storage and heterogeneous catalysis.[24-26] Porous MOFs have permanent nano-scaled cavities and open channels offering congenital conditions for small molecules to access and therefore show a potential for use as a template to synthesize nanoporous carbon materials.[27] Several MOFs, typically MOF-5 ($[Zn_4O\ (OOCC_6H_4COO)_3]$), have been demonstrated as promising templates, yielding highly nanoporous carbons revealed to be technologically important for various applications owing to their unique nature of nanoporous structures and high chemical/electrochemical durability.[27-30] More recently, some researchers investigated the chemical activation of the nanoporous carbons by KOH.[31,32] Interestingly, it was found that this activation resulted in a substantial increase of surface area and a simultaneous augment of pore volume for the activated nanoporous carbons, and the materials showed the superior electrochemical properties as precursors for supercapacitors. On the other hand, the high specific surface area is favorable for metal dispersion, and the abundant pores are also beneficial to facilitate mass transfer. Obviously, the activated nanoporous carbons have possessed the basic characteristics of an ideal carrier material. To the best of our knowledge, the activated nanoporous carbons as catalyst carriers are rarely reported in the studies of fuel cells.

Here, the NPC has been synthesized through thermolysis of MOF-5 with furfuryl alcohol (FA) as the additional carbon source and subsequently activated by KOH. The

obtained A-NPC is firstly used as an anode catalyst carrier for DBHFC. The catalytic activity of borohydride oxidation and the performance of single DBHFCs are investigated in detail.

2. Experimental

2.1. Preparation of NPC and activated NPC

The NPC was synthesized by carbonization of MOF-5 with furfuryl alcohol (FA) as carbon source.[27,28] Firstly, the MOF-5 was prepared by solvothermal method with the optimal synthesis conditions according to the literature.[33] After the as-prepared MOF-5 was degassed at 200 ^{o}C for 24 h, the FA was introduced into the pores of degassed MOF-5 via the incipient wetness technique. Secondly, thermal treatment of the FA/MOF-5 composite was performed in the tube furnace under argon atmosphere with the treatment process as follows: polymerized at 80 ^{o}C for 24 h, carbonized at 150 ^{o}C for 6 h followed by 900 ^{o}C for 6 h. The resultant nanoporous carbon was denoted as NPC.

For a typical KOH activation, the NPC sample was thoroughly mixed with KOH at a carbon/KOH mass ratio of 1/5. Then the mixture was placed in a tube furnace and the tube was Ar purged for 30 min, followed by heating the sample with a rate of 5 ^{o}C min^{-1} up to 900 ^{o}C and holding at this temperature for 60 min under flowing argon with a flow rate of 100 cm^{3} min^{-1}. Subsequently, the resulting material was washed repeatedly with 2 M hydrochloric acid and next with sufficient distilled water. Finally, the resultant sample was dried at 100 ^{o}C for 12 h. The NPC after activation was labeled as A-NPC.

2.2. Catalysts synthesis

Au nanoparticles were deposited on the NPC, A-NPC and commercial Vulcan XC-72R (XC-72, Cabot) via the means of incipient-wetness and reduction with sodium borohydride. Firstly, the required amounts of the carbon carrier, polyvinyl pyrrolidone (PVP) were mixed with 100 mL deionized water containing the Au precursor, chloroauricacid ($HAuCl_4 \cdot 4H_2O$, Aldrich). The amount of $HAuCl_4 \cdot 4H_2O$ in the solution was adjusted to obtain 20 wt.% Au loading. After the mixture vigorous stirring for 30min, 3 M NaOH solution was added to adjust the pH of the mixture to 10 and then 1 mL of 1 M $NaBH_4$ was added dropwise. Allowing the reduction of $HAuCl_4 \cdot 4H_2O$ to complete, keep additional stirring for 24 h. Finally, the mixture was filtered and rinsed with deionized water several times, then dried at 80 ^oC under vacuum for 12 h to obtain the Au/C (C=NPC, A-NPC, XC-72) electrocatalyst.

2.3. Physical characterization

The carbon carriers were characterized by physical N_2 adsorption-desorption at 77 K (using an AUTOSORB-1 instrument from Quantachrome). The estimation of the Brunauer-Emmett-Teller (BET) specific surface area, pore volume and pore size distribution were carried out according to the Barrett-Joyner-Halenda (BJH). TEM images were carried out using a JEOL JSM-2100F micro-scope operating at 200 kV. The TEM samples were prepared by placing several drops of dilute particle dispersion on carboncoated copper TEM grids. Powder XRD analyses were performed on a D/Max-3C diffractometer with Cu Kα radiation (λ=1.54056Å).

2.4. Electrochemical measurements

The electrocatalytic performance of the as-prepared catalysts was tested with a VersaSTAT3

electrochemical workstation (Princeton, America) that was connected to a standard three-electrode system. An Ag/AgCl, KCl_{std} electrode was used as a reference electrode, and a Ni foam mesh with 3 × 5 cm^2 was used as the counter electrode. The working electrode was prepared by casting 5 μL of electrocatalyst ink onto a pre-polished glassy carbon disk (GC, 3 mm in diameter). Typically, the electrocatalyst ink was prepared by sonicating 10 mg electrocatalyst in 750 μL distilled water followed by adding 250 μL Nafion (5 wt.% from Aldrich) and sonicated further to form a homogeneous ink, which was then casted on GC electrode. The dispersed electrocatalyst on the GC surface was dried at ambient temperature.

2.5. Fuel cell test

The performance of single fuel cell test was evaluated by a battery testing system (BTS-51800, Neware Technology Co. Ltd., China) at 25 ^oC. The cell was consisted of Au/XC-72 cathode, Au/C anode, pretreated Nafion 117 membrane separator, anolyte composed of 1 M $NaBH_4$ + 3 M NaOH, and catholyte composed of 2 M H_2O_2 + 0.5 M H_2SO_4. The load was applied in steps of 5 mA within the range of 0-120 mA. Each step lasted 2 min and the current was continuously applied from one value to next without disconnecting cell. The discharge current density of 20 mA cm^{-2} was applied to test the durability of cell performance.

In order to fabricate the anode or cathode, the slurry of the catalyst was prepared by mixing the catalyst, isopropyl alcohol and 7 wt.% Nafion solution. Firstly, this slurry was ultra-sonicated for 2 h and then subjected to magnetic stirring for 2h. Subsequently, the ink was coated on the stainless steel gauze and dried in an oven at 60 ^oC for 8 h. Finally, the

coated tainless steel gauze was pressed at 16 MPa for 1 min to obtain anode or cathode. The loading mass of electrocatalysts was 4-4.5 mg cm^{-2}.

3. Results and discussion

The specific surface area and microstructure of the nanoporous carbon before and after activation treatment are derived from their corresponding N_2 adsorption-desorption isotherms shown in Fig. 1 (a). Type-IV isotherms with distinct hysteresis loops are found for both NPC and A-NPC, which suggest the existence of different pore sizes spanning from micro to macropores in the two samples. It is noteworthy that the BET specific surface area of the activated sample A-NPC dramatically increases from 1123 m^2 g^{-1} of the NPC to 2296 m^2 g^{-1}, and the corresponding total pore volume rises from 0.896 cm^3 g^{-1} to 1.59 cm^3 g^{-1} as well. Moreover, it can be observed from Fig. 1 (b) that the development of high porosity is remarkably pronounced during the KOH activation, especially the small mesopores (2-4 nm). Consequently, it can be concluded that the KOH activation can further tune the porous structures and enlarge the surface area of the NPC, as anticipated.

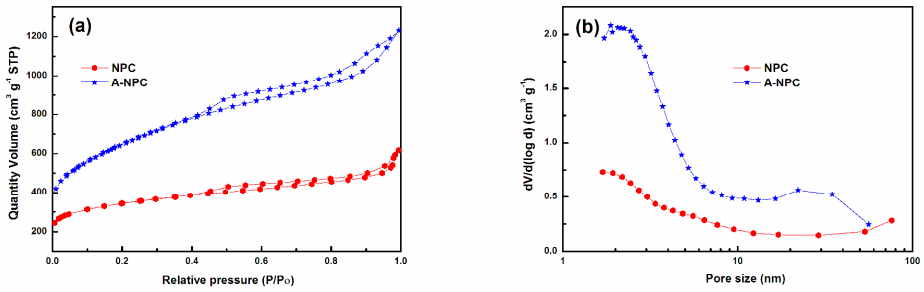

Fig. 1 (a) Nitrogen adsorption-desorption isotherms and (b) pore size distributions calculated from N_2 adsorption isothermals for NPC and A-NPC supports.

The XRD patterns of the three electrocatalysts are shown in Fig. 2. The diffraction peak at about 25° is from carbon (002), and peaks at 2θ values about 38.1°, 44.3°, 64.5°,

77.5° and 81.6° are ascribed to the Au (111), Au (200), Au (220), Au (311) and Au (222) crystal faces, respectively, representing that the Au particles deposited on XC-72, NPC and A-NPC all have typical face-centered cubic (fcc) structure. Notably, no diffraction peak of the impurity can be observed in the XRD patterns of Au/NPC and Au/A-NPC catalysts. In addition, the Au particle sizes, calculated from the Au (220) peak width using Debye-Scherrer equation[34] are about 5.1, 3.5 and 3.2 nm for Au/XC-72, Au/NPC and Au/A-NPC electrocatalysts, respectively.

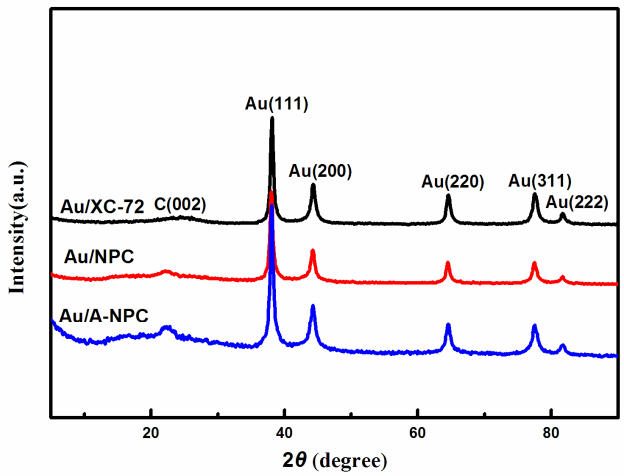

Fig. 2 XRD patterns of Au/XC-72, Au/NPC and Au/A-NPC electrocatalysts.

To further elucidate the morphologies of the electrocatalysts, the TEM images and the corresponding size distribution histograms of the Au particles have been examined. Fig. 3 (a) and 3 (c) clearly reveal that the spherical dark Au crystallites on the activated carrier A-NPC are smaller and more uniformly dispersed, contrasted to that on the untreated NPC with evident agglomeration in some areas. Consistent with the XRD results, the average sizes of Au crystallites on the A-NPC and NPC, estimated over 200 particles as shown in histograms (Fig. 3 (b) and 3 (d)), are only 2.9 and 3.1 nm. Both the two samples display

smaller particle sizes than that on Vulcan XC-72R (5.2 nm) reported in our previous work[35]. From close observation, it can also be seen that the size dispersion of Au crystallites is the narrowest on the A-NPC. These results indicate that the A-NPC with high specific surface area as carrier can further improve the dispersion of Au particles and inhibit their aggregation. In other words, an accessible and sufficiently large surface for maximum catalyst dispersion is necessary.

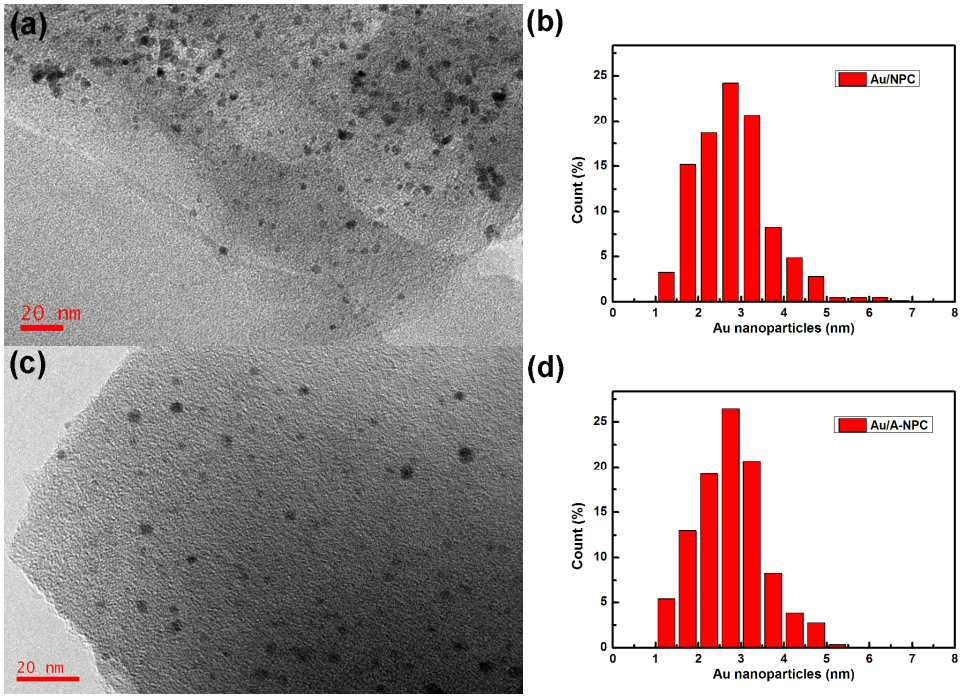

Fig. 3 TEM images of (a) Au/NPC and (c) Au/A-NPC, and Au particle size distribution histograms of (b) Au/NPC and (d) Au/A-NPC.

The cyclic voltammetry curves using the Au/XC-72, Au/NPC and Au/A-NPC electrodes in a solution containing 0.1 M $NaBH_4$ and 3 M NaOH at a scan rate of 20 mV s^{-1} in the potential range of -1.2 V to 0.6 V vs. Ag/AgCl, KCl_{std} are shown in Fig.4. As seen, the CV curves characterized by several oxidation peaks are in accordance with the reported results.[36-38] For all electrocatalysts, in the forward scan, a well-defined oxidation peak

appearing in the potential range between -0.4 V and -0.15 V is considered to be the direct oxidation of borohydride. During the subsequent return scan under the potential region from 0.0 to 0.4 V, a sharp peak is observed, which can be attributed to the oxidation of adsorbed species such as BH_3OH^- or other borohydrides formed as an intermediate during the oxidation of the BH_4^- in the forward scan.

Generally, the direct oxidation peak potential and peak current density of BH_4^- are used as a metric to establish a quantitative comparison of catalyst activity. Apparently, the Au/A-NPC electrocatalyst reveals the highest peak current density of BH_4^- oxidation (49.1 mA cm^{-2}), which is 13.6% higher than that of Au/NPC (43.2 mA cm^{-2}), and 63.1% higher than that of Au/XC-72 (30.1 mA cm^{-2}). Additionally, the oxidation peak potential of BH_4^- for Au/A-NPC electrocatalyst is ca 0.20 V more negative compared to both the Au/NPC and Au/XC-72 electrocatalysts, indicating that borohydride electro-oxidation is kinetically more favorable on Au/A-NPC electrocatalyst. From these results it can be found that the Au/A-NPC electrocatalyst possesses a higher electrocatalytic activity for borohydride electro-oxidation than Au/NPC and Au/XC-72 electrocatalysts.

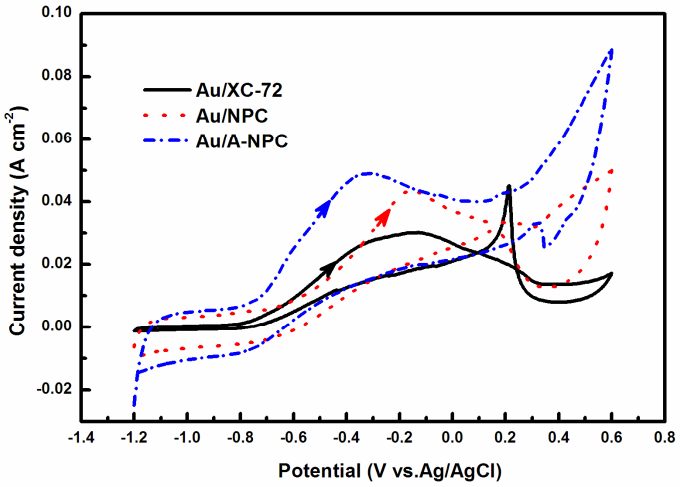

Fig. 4 Cyclic voltammograms for the electro-oxidation of BH_4^- in a 0.1 M $NaBH_4$ + 3 M NaOH solution for the Au carbon-supported catalysts. Scan rate: 20 mV s^{-1}.

Chronoamperograms can give clues about electrocatalyst stability in fuel cells. Fig. 5 presents the typical test results of Au/XC-72, Au/NPC and Au/A-NPC electrocatalysts. As seen, the initial current density is the highest on Au/A-NPC (0.413 mA cm^{-2}), followed by Au/NPC (0.406 mA cm^{-2}) and Au/XC-72 (0.398 mA cm^{-2}). At the end of experimental period (t = 1000 s), the residual current density of Au/A-NPC, Au/NPC and Au/XC-72 are 0.0192 mA cm^{-2}, 0.0127 mA cm^{-2} and 0.0099 mA cm^{-2}, respectively. Obviously, the current density decay of Au/A-NPC is much slower than that on the Au/NPC and Au/XC-72 electrocatalysts, suggesting that the order of catalytic activity and stability for the three electrodes is Au/A-NPC > Au/NPC > Au/XC-72, which is in good agreement with the results of CV curves as shown in Fig.4.

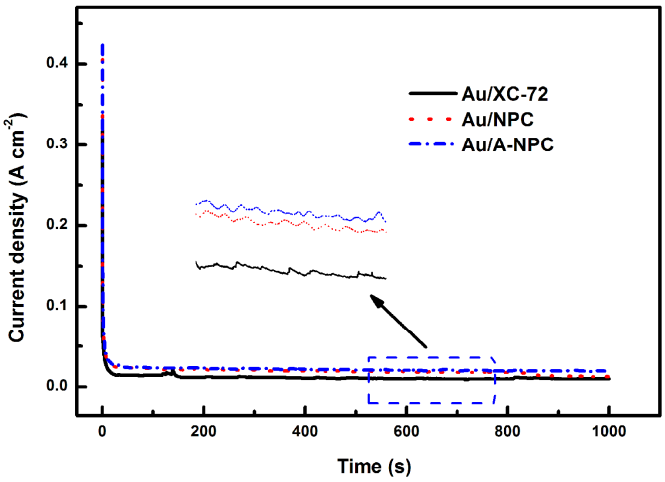

209

210 Fig. 5 Chronoamperometry curves of electrooxidation $NaBH_4$ on different electrodes in 0.1M $NaBH_4$ + 3

211 M NaOH solution.

212 Chronopotentiometry is another useful method for screening electrocatalyst since it

213 can simulate the constant current operation of a DBHFC. The CP experiments are

214 performed for the anode catalysts at an applied current density step of 8.5 mA cm^{-2} to the

215 electrode for 120 s. It can be clearly seen from Fig. 6 that the operating potentials for

216 Au/A-NPC is up to about 0.145 V more negative than Au/NPC, and 0.298 V than

217 Au/XC-72 after 120s, demonstrating that the overpotential for the oxidation of BH_4^- ions

218 on the former catalyst is lower than that on the Au/NPC and Au/XC-72 electrocatalysts. A

219 lower overpotential is known to be an indication of better electroactivity. Accordingly, the

220 Au/A-NPC electrocatalyst can behave higher electro-oxidation activity and power output

221 than those on Au/NPC and Au/XC-72 electrocatalysts.

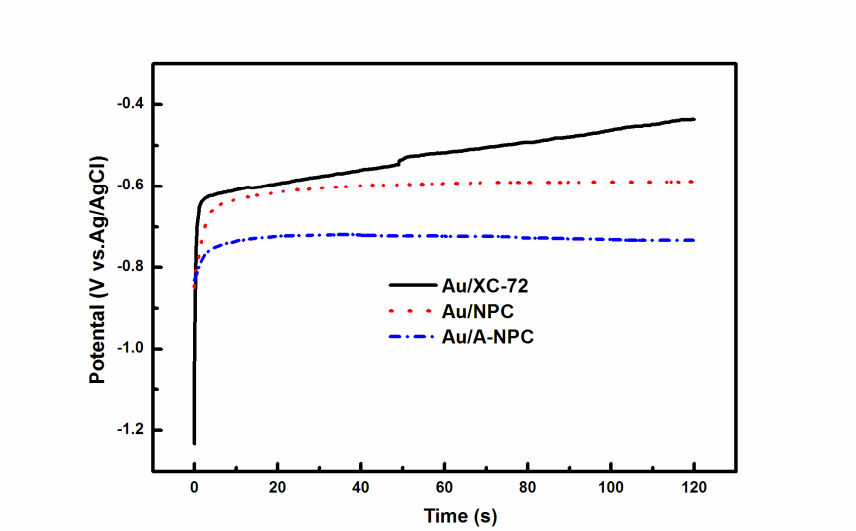

Fig. 6 Chronopotentiometry results for BH_4^- oxidation on different electrodes in 0.1 M $NaBH_4$ + 3 M NaOH solution. Current step was from 0 to 8.5 mA cm^{-2}.

The results from the voltammetric performance, chronoamperometry and chronopotentiometry confirm that the A-NPC as alternative to commercial carbon Vulcan XC-72 can enhance the catalytic activity of borohydride electro-oxidation and simultaneously improve the stability of catalyst. Regarding the reasons for this phenomenon, the significantly large specific surface area and well-developed porous structure of the A-NPC are supposed to be responsible for the enhanced activity and durability of the catalyst. Since these unique characteristics above can augment the adsorbability of the catalyst and extend the active area, result in excellent electrocatalytic activity performances. Therefore the A-NPC is a robust carrier for electrocatalyst in fuel cell.

Fuel cell experiments are carried out at 25 ^oC using Au/NPC, Au/A-NPC and Au/XC-72 as anode catalysts and Au/XC-72 as cathode catalyst equipped with Nafion 117 membrane. Fig. 7 displays the polarization and power density curves of the single DBHFCs

operating with 1 M $NaBH_4$ and 3 M NaOH as a fuel and hydrogen peroxide as oxidant. The values of OCV are approximately 1.75 V, which are much lower than the theoretical OCV of DBHFC (3.01 V). The deviation is mainly due to the formation of the mixed potentials by both BH_4^-/BO_2^- and H_2O/H_2 couples at open voltage.[39] It is evident that the cell voltage of Au/A-NPC anode catalyst drops much more slowly with the increase of current density than Au/NPC and Au/XC-72 anode catalysts under identical conditions. Furthermore, the maximum power density of the DBHFC employing the Au/A-NPC anode catalyst is as high as 48.2 mW cm^{-2} at 59.7 mA cm^{-2}. While in the case of the single cells with Au/NPC and frequent Au/XC-72 anodes, the corresponding maximum power densities are only 38.8 and 19.9 mW cm^{-2}, respectively. The improvement in the cell performance is most likely to be ascribed to the uniform dispersion with a smaller particle size of the Au nano-crystallites deposited on the A-NPC, as well as the abundant mesoporous of the A-NPC which is beneficial to facilitate mass transfer. Therefore, the single cell tests demonstrate once again that the A-NPC is an excellent catalyst carrier for DBHFC.

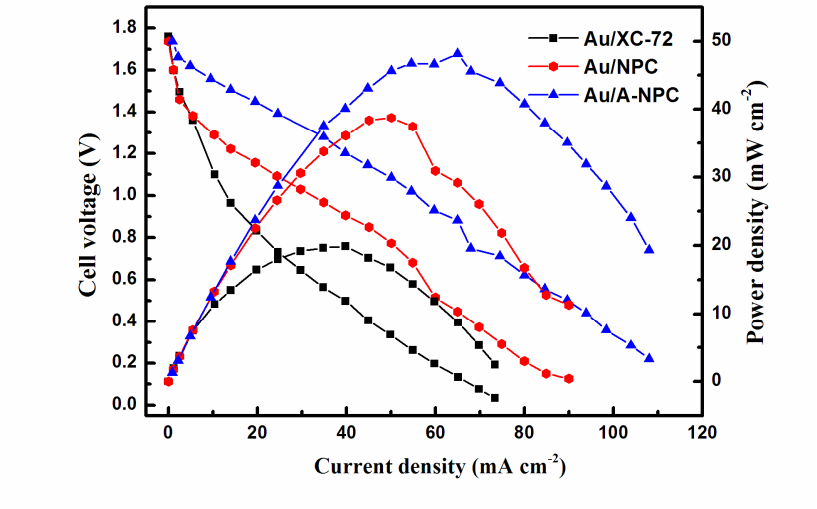

Fig. 7 Cell voltage and power density *vs*. current density for DBHFCs with different anodes at 25 °C.

Anolyte: 1 M $NaBH_4$ + 3 M NaOH; catholyte: 2 M H_2O_2 + 0.5 M H_2SO_4. Catalyst loading: 4- 4.5 mg cm^{-2}.

In the view of practical application, the durability of the materials under fuel cell conditions is particularly important. Fig. 8 shows the result of the short-term stability test for the anode catalysts, which is measured by monitoring the cell voltage change during the galvanostatic discharge of 20 m A cm^{-2} at 25 ^{o}C. It can be observed that the Au/A-NPC anode maintains a relatively stable performance for a period of about 24 h in the case of fuel limited. However, the Au/XC-72 anode shows a rapid decrease in performance and stability in 20 h. Besides, the cell voltage of DBHFC with the Au/A-NPC anode is higher than that of Au/XC-72 anode over the test period. As a consequence, the Au/A-NPC anode possesses a good short-term stability.

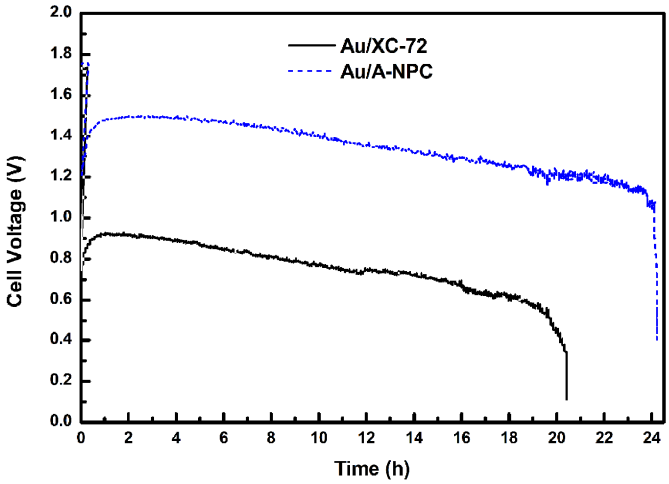

Fig. 8 Performance stability of the DBHFCs operating at current density of 20 mA cm^{-2} at 25 ^{o}C. Anode: Au/A-NPC and Au/XC-72. Fuel: 50 ml 1 M $NaBH_4$ + 3 M NaOH.

4. Conclusion

In the present study, the A-NPC has been synthesized via KOH activation of NPC and successfully utilized as a catalyst carrier of Au nanoparticles in anode of DBHFC for the first time. Textural characterization of the A-NPC reveals high specific surface areas about 2296 $m^2 g^{-1}$ with an important contribution of mesoporous. It is important to emphasize that the spherical Au crystallites on the A-NPC are smaller and more uniformly dispersed, contrasted to that on the NPC and commercial carbon Vulcan XC-72. In addition, the Au/A-NPC catalyst exhibits a lower peak potential and significantly higher current density of 49.1 mA cm^{-2} for BH_4^- electro-oxidation than Au/NPC and Au/XC-72 catalysts. Also, in single cell tests, the Au/A-NPC catalyst shows a markedly superior power density to other two catalysts. Apparently, the improvement in electrocatalytic activity of the anode catalyst is achieved via using the A-NPC as carrier. Hence, the A-NPC with unique characteristics can be considered as a promising anode catalyst carrier for the application of DBHFC.

Acknowledgements

This work was financially supported by the National Natural Science Foundation of China (Grant Nos. 51272221, 51072173 and 21203161), Natural Science Foundation of Hunan Province, China (Grant No. 13JJ4051), Scientific Research Fund of Hunan Provincial Education Department (Grant No. 11A118), and Universities in Hunan Province plans to graduate research and innovation under project (Grant No. 20134301130001).

Reference

1 U. B. Demirci and P. Miele, *Energy Environ. Sci.*, 2009, 2, 627-637.

2 B. M. Concha, M. Chatenet, F. Maillard, E. A. Ticianelli, F. H. B. Lima and R. B. de Lima, *Phys. Chem. Chem. Phys.*, 2010, 12, 11507-11516.

3 R. L. Arevalo, M. C. S. Escaño and H. Kasai, *ACS Catal.*, 2013, 3, 3031-3040.

4 H. Y. Qin, L. B. Jiang, Y. C. He, J. B. Liu, K. Cao, J. Wang, Y. He, H. Ni, H. Z. Chi and Z. G. Ji, *J. Mater. Chem. A*, 2013, 1, 15323-15328.

5 N. A. Choudhury, R. K. Raman, S. Sampath and A. K. Shukla, *J. Power Sources*, 2005, 143, 1-8.

6 G. H. Miley, N. Luo, J. Mather and R. Burton, *J. Power Sources*, 2007, 165, 509-16.

7 J. Ma, N. A. Choudhury and Y. Sahai, *Renewable Sustainable Energy Rev.*, 2010, 14, 183-199.

8 W. J. Paschoalino and E. A. Ticianelli, *Int. J. Hydrogen Energy*, 2013, 38, 7344-7352.

9 G. Rostamikia and M. J. Janik, *Energy Environ. Sci.*, 2010, 3, 1262-1274.

10 P. Y. He, X. Y. Wang, Y. J. Liu, L. H. Yi and X. Liu, *Int. J. Hydrogen Energy*, 2012, 37, 1254-1262.

11 Y. K. Zhou, K. Neyerlin, T. S. Olson, S. Pylypenko, J. Bult, H. N. Dinh, T. Gennett, Z. P. Shao and R. O'Hayre, *Energy Environ. Sci.*, 2010, 3, 1437-1446.

12 C. Alegre, M. E. Gálvez, E. Baquedano, R. Moliner, E. Pastor and M. J. Lázaro, *J. Phys. Chem. C*, 2013, 117, 13045-13058.

13 J. Y. Cheon, C. Ahn, D. J. You, C. Pak, S. H. Hur, J. Kim and S. H. Joo, *J. Mater. Chem. A*, 2013, 1, 1270-1283.

14 L. An, T. S. Zhao, Y. S. Li and Q. X. Wu, *Energy Environ. Sci.*, 2012, 5, 7536-7538.

15 W. M. Zhang, P. Sherrell, A. I. Minett, J. M. Razal and J. Chen, *Energy Environ. Sci.*,

2010, 3, 1286-1293.

16 J. L. Figueiredo and M. F. R. Pereira, *J. Energy Chem.*, 2013, 22, 195-201.

17 W. Z. Li, M. Waje, Z. W. Chen, P. Larsen and Y. S. Yan, *Carbon*, 2010, 48, 995-1003.

18 A. Marinkas, F. Arena, J. Mitzel, G. M. Prinz, A. Heinzel, V. Peinecke and H. Natter, *Carbon*, 2013, 58, 139-150.

19 A. Kumar and V. K. Ramani, *Appl. Catal. B*, 2013, 138-139, 43-50.

20 G. Q. Xia, C. D. Huang and Y. X. Wang, *Int. J. Hydrogen Energy*, 2013, 38, 13754-13761.

21 M. Ghasemi, S. Shahgaldi, M. Ismail, B. H. Kim, Z. Yaakob and W. R. Wan Daud, *Int. J. Hydrogen Energy*, 2011, 36, 13746-13752.

22 A. E. Aksoylu, M. Madalena, A. Freitas, M. F. R. Pereira and J. L. Figueiredo, *Carbon*, 2001, 39, 175-185.

23 A. Nieto-Márquez, V. Jiménez, A. M. Raboso, S. Gil, A. Romero and J. L. Valverde, *Appl. Catal. A*, 2011, 393, 78-87.

24 H. L. Li, M. Eddaoudi, M. O'Keeffe and O. M. Yaghi, *Nature*, 1999, 402, 276-279.

25 S. Q. Ma and H.-C. Zhou, *Chem. Commun.*, 2010, 46, 44-53.

26 M. L. Aubrey, R. Ameloot, B. M. Wiers and J. R. Long, *Energy Environ. Sci.*, 2014, DOI: 10.1039/C3EE43143F.

27 B. Liu, H. Shioyama, T. Akita and Q. Xu, *J. Am. Chem. Soc.*, 2008;130:5390-5391.

28 B Liu, H Shioyama, H. L. Jiang, X. B. Zhang and Q. Xu, *Carbon*, 2010, 48, 456-463.

29 M. Hu, J. Reboul, S. Furukawa, N. L. Torad, Q. M. Ji, P. Srinivasu, K. Ariga, S. Kitagawa and Y. Yamauchi, *J. Am. Chem. Soc.*, 2012, 134, 2864-2867.

30 N. L. Torad, M. Hu, Y. Kamachi, K. Takai, M. Imura, M. Naito and Y. Yamauchi, *Chem. Commun.*, 2013, 49, 2521-2523.

31 J. Hu, H. L. Wang, Q. M. Gao and H. L. Guo, *Carbon*, 2010, 48, 3599-3606.

32 A. Almasoudi and R. Mokaya, *J. Mater. Chem.*, 2012, 22, 146-152.

33 J. P. Li, S. J. Cheng, Q. Zhao, P. P. Long and J. X. Dong, *Int. J. Hydrogen Energy*, 2009, 34, 1377-1382.

34 L. G. R. A. Santos, C. H. F. Oliveira, I. R. Moraes and E. A. Ticianelli, *J. Electroanal. Chem.*, 2006, 596, 141-148.

35 P. Y. He, X. Y. Wang, P. Fu, H. Wang and L. H. Yi, *Int. J. Hydrogen Energy*, 2011, 36, 8857-8863.

36 E. Gyenge, *Electrochim. Acta*, 2004, 49, 965-978.

37 D. M. F. Santos and C. A. C. Sequeira, *Electrochim. Acta*, 2010, 55, 6775-6781.

38 M. Chatenet, F. H. B. Lima and E. A. Ticianelli, *J. Electroanal. Chem.*, 2010, 157, B697-B704.

39 C. Ponce de León, F. C. Walsh, C. J. Patrissi, M. G. Medeiros, R. R. Bessette, R. W. Reeve, J. B. Lakemanc, A. Rosec and D. Browning, *Electrochem. Commun.*, 2008, 10, 1610-1613.